Wave based modelling of enclosed spaces by a sequence of matrix multiplications

Rob Opdam, Diemer de Vries, Michael Vorländer

ACOUSTICS 2012

Wave based modelling of enclosed spaces by a sequence of matrix multiplications

R. C. Opdam, D. De Vries and M. Vorländer

RWTH Aachen University, Institute of Technical Acoustics, Neustrasse 50, 52066 Aachen, Germany
rob.opdam@akustik.rwth-aachen.de

In room acoustical planning it is important to obtain realistic impulse responses from simulations to calculate the well-known room acoustical parameters as reverberation time, clarity etc. In most cases this is done by using a hybrid implementation of ray-tracing and mirror image sources. This paper presents a method adopted from the field of seismic imaging, which is based on the concept of wave field extrapolation. The advantage of modelling with the full wave character of sound propagation is that all physical phenomena can be simulated correctly (e.g. diffraction from edges). The proposed algorithm uses a sequence of matrix multiplications that represent generalised spatial convolutions. The matrices give ample insight in the physical processes, like propagation, non-locally reacting (complex) reflection properties and absorption. The algorithm is theoretically able to solve for an infinite number of reflections. A comparison is made with conventional methods. Therefore, a simple rectangular box with uniform walls and a three-dimensional configuration of an L-shaped wall, placed in an anechoic environment, are simulated. The L-shaped wall is firstly covered with a hard surface and secondly with a non-locally reacting absorber.

1 Introduction

The computational modelling of acoustical fields in enclosed spaces (rooms) is in practise done with algorithms based on the mirror image source model (MISM) [1], the ray tracing model (RTM) [2] or a mixture of both (hybrid method) [3]. In the most common hybrid solutions the first reflections (specular components) are calculated by the mirror image source method and the later reflections (scattered components) by the ray tracing method.

Those two methods are not capable of dealing with diffraction (non-specular components) in general [4]. Including diffraction is important from a listeners point of view and in the calculation of room acoustical parameters especially the early decay time (*EDT*), clarity (*C*), definition (*D*) and the lateral energy fraction (*LEF*), which strongly depend on the early part of the room impulse response (RIR) [5, 6]. Therefore, extensions are developed to add edge diffraction to MISM [7, 8]. In adding diffraction, for instance by Pierce's method for MISM [7],The average value over time and space is sufficient for most room acoustical parameters, but not at the individual listeners positions [6, 9]. Round robin tests of room acoustical computer simulations has pointed out that there is room for improvement of the predictions [10, 11].

Another difficult part is the description of the boundary properties. With the previous described methods it is partly (or not) possible to define boundary impedance properties [4]. The influence of such complex boundaries is not yet explored in room acoustics. Another aspect that could be present in non-rigid boundaries is the non-locally reacting effect of a boundary. Other wave based methods as boundary element (BEM) and finite element methods (FEM) are capable of handling these complex boundary conditions, but are very computationally demanding and therefore not used for large scale problems.

In this paper a wave field extrapolation method is described, that is derived from an algorithm that is widely applied in seismic exploration [12]. This seismic algorithm is called the WRW model, where the W stands for wave propagation and the R for reflection [13]. The model is most similar to BEM methods. The advantage of this model is that it is a wave based method, which therefore includes all physical phenomena of sound propagation and reflection. The model has already been implemented for 2-D simulations [14]. In this paper a further developed model is presented, which includes 3-D capabilities and the implementation of non-locally reacting boundaries.

2 Wave field extrapolation

The underlying theory of the WRW method starts with the Huygens principle. Huygens stated that a propagating wave in a homogeneous medium can be described by adding all contributions of secondary sources positioned along a wavefront. This interpretation was later quantitatively derived and described by the Kirchhoff-Helmholtz integral:

$$P(\vec{r}_A,\omega) = \frac{1}{4\pi}\oint_S \Bigg[\overbrace{j\omega\rho_0 V_n(\vec{r}_S,\omega)\frac{e^{-jk\Delta r}}{\Delta r}}^{\text{weighted monopole field}} + \underbrace{P(\vec{r}_S,\omega)\frac{1+jk\Delta r}{\Delta r}\cos(\phi)\frac{e^{-jk\Delta r}}{\Delta r}}_{\text{weighted dipole field}} \Bigg] dS \quad (1)$$

where $\Delta r = |\vec{\Delta r}| = |\vec{r}_A - \vec{r}_S|$ is the distance from a secondary source point on the boundary S and the reconstruction point A within the enclosed volume V, ϕ is the angle between the normal vector $\vec{n}$ pointing inward to the volume and the vector $\vec{\Delta r}$ between a secondary source and the reconstruction point, V_n is the particle velocity in the normal inward direction, P the pressure, wavenumber k is defined as the angular frequency ω divided by the propagation velocity c and ρ_0 is the air density. With the Kirchhoff-Helmholtz equation as given in Eq. (1) it is possible to predict the pressure anywhere in the source free volume V if the normal particle velocity and pressure are known everywhere at the boundary S as indicated in Figure 1. In the derivation of the Kirchhoff-Helmholtz integral (see [13] for the full details) it is possible to expand the Green's function for a homogeneous medium linearly with an arbitrary solution of the source free Helmholtz equation, say $\Gamma(\vec{r},\omega)$. This solution $\Gamma(\vec{r},\omega)$ can be chosen in such a way that the dipole or monopole term in Eq. (1) is cancelled

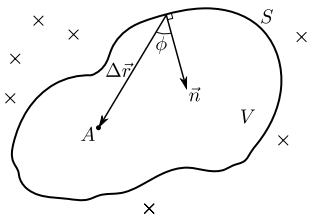

Figure 1: Primary sources (×) and volume V and boundary S for the Kirchhoff-Helmholtz integral equation.

out. These two solutions are given as:

$$\Gamma_1(\vec{r},\omega) = \frac{e^{jk\Delta r}}{-\Delta r} \quad (2)$$

$$\Gamma_2(\vec{r},\omega) = -\frac{e^{-jk\Delta r}}{\Delta r} \quad (3)$$

where the subscripts 1 and 2 point out that respectively the monopole or the dipole term in Eq. (1) drops out. These particular solutions are only valid for all cases if the boundary S of the volume V has specific conditions. In this particular case the volume V will be enclosed by a boundary S, which is divided in two parts S_0 and S_1. S_1 is characterised as an infinite plane and on top of that a half-space S_0 that is infinitely far away as shown in Figure 2. The primary sources are all lo-

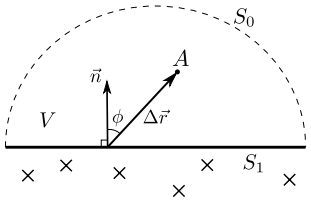

Figure 2: Volume and boundary for the Rayleigh integral equation.

cated below the infinite plane in such a way that there is only a contribution of secondary sources at the boundary part S_1. The infinite half-space S_0 has no secondary source contribution and can therefore be left out of the integration surface. In this case the pressure at any point within the volume V can be described by the knowledge of whether the pressure or the normal particle velocity along the boundary S_1. This results in the following two equations to describe the pressure at a certain point A in the volume:

$$P(\vec{r}_A,\omega) = \frac{j\omega\rho_0}{2\pi}\iint_{S_1}\left[V_n(\vec{r}_S,\omega)\frac{e^{-jk\Delta r}}{\Delta r}\right]dS_1 \quad (4)$$

$$P(\vec{r}_A,\omega) = \frac{jk}{2\pi}\iint_{S_1}\left[P(\vec{r}_S,\omega)\frac{1+jk\Delta r}{\Delta r}\cos(\phi)\frac{e^{-jk\Delta r}}{\Delta r}\right]dS_1 \quad (5)$$

where Eq. (4) is called the Rayleigh-I integral and Eq. (5) the Rayleigh-II. The method described in this paper makes use of the Rayleigh-II integral equation. In fact this equation allows to extrapolate a wave field to a further point in space if the pressure at the boundary is known.

2.1 WRW model

When an extrapolation in space from a plane at z_0 to a plane at z_1 is performed as in Figure 3, the Rayleigh-II equation can be expressed as:

$$P(x_1,y_1,z_1,\omega) = \iint_{-\infty}^{+\infty} W(\Delta x,\Delta y,\Delta z,\omega)\times P(x,y,z_0,\omega)dxdy \quad (6)$$

where $\Delta x = |x_1 - x|$, $\Delta y = |y_1 - y|$ and $\Delta z = |z_1 - z_0|$. In fact this represents a spatial convolution in x and y with $W(\Delta x,\Delta y,\Delta z,\omega)$ as integral kernel that represents the propagation from each point on the z_0 plane to the z_1 plane. The propagation kernel is defined as:

$$W(\Delta x,\Delta y,\Delta z,\omega) = \frac{jk}{2\pi}\left(\frac{1+jk\Delta r}{\Delta r}\right)\cos(\phi)\frac{e^{-jk\Delta r}}{\Delta r} \quad (7)$$

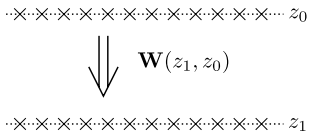

Figure 3: Spatially discretised geometry for extrapolation of the wave field from a plane at $z = z_0$ to a plane $z = z_1$.

In numerical simulations it is necessary to perform a discretisation step and the spatial convolution, as defined in Eq. (6), can then be expressed as:

$$\vec{P}(z_1) = \mathbf{W}(z_1,z_0)\vec{P}(z_0) \quad (8)$$

where the pressure is calculated for one frequency at all the points at the $z = z_1$ plane. Keep in mind that if the propagation is reversed, so extrapolation from the plane $z = z_1$ to $z = z_0$, the propagation matrix $\mathbf{W}(z_1,z_0)$ has to be inverted. The new propagation operator can be defined as $\mathbf{W}(z_0,z_1) = [\mathbf{W}(z_1,z_0)]^T$. Another important process of wave propagation is the reflection at a boundary. In case of a geometry with one boundary at $z = z_1$, the incoming wave field $\vec{P}^+(z_1)$ and the reflected wave field $\vec{P}^-(z_1)$, as drawn in Figure 4, can be expressed as:

$$\vec{P}^-(z_1) = \mathbf{R}(z_1)\vec{P}^+(z_1) \quad (9)$$

where the reflection matrix $\mathbf{R}(z_1)$ is defined as a diagonal

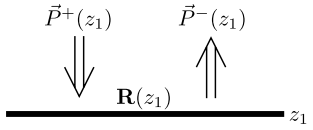

Figure 4: Reflection of a wave field at a boundary.

matrix with the reflection coefficients of each grid point on the boundary for the non-locally reacting case. The reflection coefficient is defined as $R = \sqrt{1-\alpha(\omega)}$, with $\alpha(\omega)$ the absorption coefficient of the boundary. The reflection coefficients can be complex valued in case of, for instance, porous absorber material.

To make the process of propagation from a source to a boundary, reflection, and propagation from the boundary to a detector complete, the two previous processes are merged together. The source(s) can be described by the source vector $\vec{S}(z_s)$ at a certain plane $z = z_s$, the propagation from the source(s) to the boundary by the propagation matrix $\mathbf{W}(z_b,z_s)$, the reflection process by the reflection matrix $\mathbf{R}(z_b)$ and as last step the propagation from the boundary to the detector(s) by $\mathbf{W}(z_d,z_b)$. This process is schematically shown in Figure 5. The resulting sound pressure at the detector is given by:

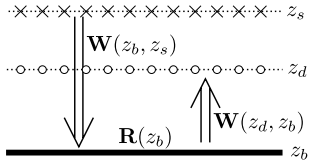

Figure 5: Propagation from sources (×) to boundary to detectors (○).

$$\begin{aligned}\vec{P}(z_d) &= \vec{P}^+(z_d) + \vec{P}^-(z_d)\\ &= \mathbf{W}(z_d,z_s)\vec{S}(z_s) +\\ &\quad [\mathbf{W}(z_d,z_b)\mathbf{R}(z_b)\mathbf{W}(z_b,z_s)]\,\vec{S}(z_s)\end{aligned} \quad (10)$$

which is known in the field of seismic exploration as the WRW model.

2.2 WRW for multiple boundaries

In the previous section the WRW method is derived for one reflection at one boundary. In this section the basic model is extended to multiple boundaries and multiple reflections to be able to simulate an enclosed space. To get a better overview over the matrix operations the notation is slightly changed. The lower indices of the matrices indicate the propagation direction, for example $\mathbf{W}(z_d, z_s)$ is indicated as $\mathbf{W}_{ds}$ for the propagation of the source(s) to the detector(s), or the boundary they are working on, for example $\mathbf{R}(z_1)$ is indicated as $\mathbf{R}_{b_1}$. This also takes away the restriction that the propagation can only take place between parallel planes. The orientation of the boundaries is unrestricted and does not even have to be closed. The example case that is used is a rectangular room with four sidewalls (boundaries b_1 to b_4), a ceiling (boundary b_5) and a floor (boundary b_6), which also encloses sources (s_1 and s_2) and detectors (d_1 to d_4). 2-D cross section of this geometry is given in Figure 6. The contribution to

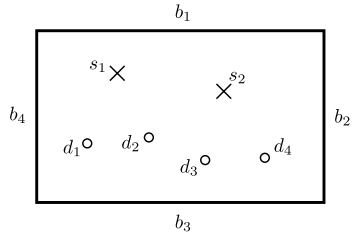

Figure 6: Rectangular room with walls (boundaries), sources (×) and detectors (○).

the wave field by the reflective part can be defined as an iterative process, which starts with propagation from the source(s) to the walls followed by a reflection and propagation to the other walls and finally contributes to the detector point(s). The calculation of the reflected wave field is schematically shown in the top part of Figure 7. The matrix operators that

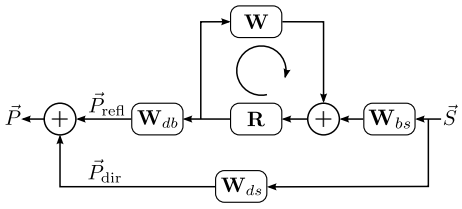

Figure 7: Diagram of the model with the total $\vec{P}$, reflected $\vec{P}_{\text{refl}}$ and direct wave field $\vec{P}_{\text{dir}}$.

include all the reflection and propagation properties for the complete geometry will be defined as follows. The source vector $\vec{S}$ includes the number of sources and their strength for the specific frequency ω and is defined as (with the total number of sources i):

$$\vec{S} = \begin{pmatrix} S_1(\omega) & S_2(\omega) & \cdots & S_i(\omega) \end{pmatrix}^T. \tag{11}$$

The matrix operator for the propagation from source(s) to detector(s) $\mathbf{W}_{ds}$, source(s) to the boundaries $\mathbf{W}_{bs}$ and boundaries to the detector(s) $\mathbf{W}_{db}$ are defined as (with the total number of sources, detectors and/or boundaries indicated as i and j):

$$\mathbf{W}_{xy} = \begin{pmatrix} W_{x_1y_1} & W_{x_1y_2} & \cdots & W_{x_1y_i} \\ W_{x_2y_1} & W_{x_2y_2} & \cdots & W_{x_2y_i} \\ \vdots & \vdots & \ddots & \vdots \\ W_{x_jy_1} & W_{x_jy_2} & \cdots & W_{x_jy_i} \end{pmatrix}. \tag{12}$$

The boundary properties are collected in one matrix $\mathbf{R}$, where on the diagonal the matrices of separate boundary properties $\mathbf{R}_b$, as mentioned in the previous section, are placed:

$$\mathbf{R} = \begin{pmatrix} \mathbf{R}_{b_1} & \mathbf{0} & \cdots & \mathbf{0} \\ \mathbf{0} & \mathbf{R}_{b_2} & & \vdots \\ \vdots & & \ddots & \vdots \\ \mathbf{0} & \cdots & \cdots & \mathbf{R}_{b_N} \end{pmatrix}. \tag{13}$$

Propagation between boundaries is collected in the matrix $\mathbf{W}$, which includes the individual propagations between the boundary parts (with N the total number):

$$\mathbf{W} = \begin{pmatrix} \mathbf{W}_{b_1b_1} & \mathbf{W}_{b_1b_2} & \cdots & \mathbf{W}_{b_1b_N} \\ \mathbf{W}_{b_2b_1} & \mathbf{W}_{b_2b_2} & & \vdots \\ \vdots & & \ddots & \vdots \\ \mathbf{W}_{b_Nb_1} & \cdots & \cdots & \mathbf{W}_{b_Nb_N} \end{pmatrix}, \tag{14}$$

the matrix components $\mathbf{W}_{pp}$ represent the interaction of the boundary with itself. This can be interpreted as propagating bending waves. In general cases these matrices will be zero $\mathbf{W}_{pp} = \mathbf{0}$. Furthermore, it can be easily seen that $\mathbf{W}_{pq} = \mathbf{W}_{qp}$.

Analogue to Eq. (10), the reflected wave field at the detector location(s) in case of one reflection with multiple boundaries is calculated by:

$$\vec{P}_1 = [\mathbf{W}_{db}\mathbf{R}\mathbf{W}_{bs}]\,\vec{S} \tag{15}$$

and if this is extended to the m^{th}-order reflection the expression in Eq. (15) can be generalised to:

$$\vec{P}_m = [\mathbf{W}_{db}\,(\mathbf{R}\mathbf{W})^m\,\mathbf{R}\mathbf{W}_{bs}]\,\vec{S} \tag{16}$$

The resulting reflected wave field at the detector locations $\vec{P}_{\text{refl}}$ is given by the summation of all reflection orders M, which gives the following expression in case $M = \infty$:

$$\begin{aligned} \vec{P}_{\text{refl}} &= \sum_{m=0}^{\infty} [\mathbf{W}_{db}\,(\mathbf{R}\mathbf{W})^m\,\mathbf{R}\mathbf{W}_{bs}]\,\vec{S} \\ &= \left[\mathbf{W}_{db}\,(\mathbf{I} - \mathbf{R}\mathbf{W})^{-1}\,\mathbf{R}\mathbf{W}_{bs}\right]\vec{S} \end{aligned} \tag{17}$$

where use is made of the fact that the summation is a Neumann series, which can be written as a matrix inversion. The matrix $\mathbf{I}$ here is the unity matrix. Furthermore, it is necessary to add the direct wave field $\vec{P}_{\text{dir}}$ from the source(s) to the detector(s) to get the total wave field $\vec{P}$ at the detector(s), schematically shown in the bottom part of Figure 7. The total wave field is therefore given by:

$$\begin{aligned} \vec{P} &= \vec{P}_{\text{dir}} + \vec{P}_{\text{refl}} \\ &= \left[\mathbf{W}_{ds} + \mathbf{W}_{db}\,(\mathbf{I} - \mathbf{R}\mathbf{W})^{-1}\,\mathbf{R}\mathbf{W}_{bs}\right]\vec{S} \end{aligned} \tag{18}$$

2.3 Non-locally reacting reflection

The structure of the matrix with the boundary properties $\mathbf{R}_b$ allows to incorporate non-locally reacting (or angle dependent) reflection properties. Each row in the $\mathbf{R}_b$ matrix can be interpreted as a reflectivity convolution operator [15]. In case of a locally reacting surface the convolution operator is represented by a finite impulse in the space-frequency domain and give unity in the angle-frequency domain as shown in Figure 8. The transformation between the two domains is by means of a spatial Fourier transform, where $k_x = \frac{\omega}{c} \sin\alpha$, with α the angle of incidence. The reflection matrix is for

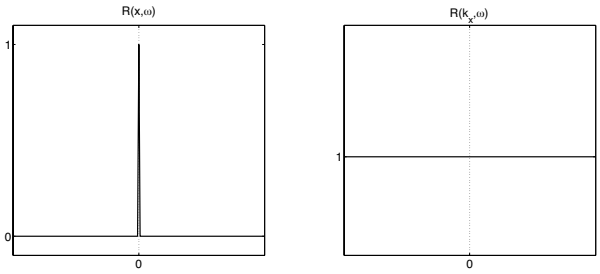

Figure 8: Locally reacting reflection in space-frequency $R(x, \omega)$ and angle-frequency $R(k_x, \omega)$ domain.

the locally reacting case a diagonal matrix with the reflection coefficients on the diagonal:

$$\mathbf{R}_b = \begin{pmatrix} R(\omega) & 0 & \cdots & 0 \\ 0 & R(\omega) & & \\ \vdots & & \ddots & \vdots \\ 0 & & \cdots & R(\omega) \end{pmatrix}. \tag{19}$$

In case of a non-locally reacting boundary the convolution operator is represented as a function, for example only reflection for small angles and no reflection at wider angles (block function) as given in Figure 9. The reflection matrix

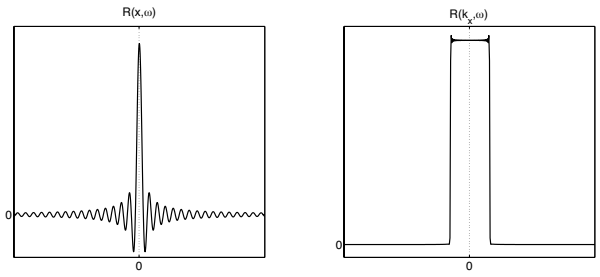

Figure 9: Non-locally reacting reflection in space-frequency $R(x, \omega)$ and angle-frequency $R(k_x, \omega)$ domain.

is defined in this case by a band matrix:

$$\mathbf{R}_b = \begin{pmatrix} R(x_{11}, \omega) & R(x_{12}, \omega) & \cdots & 0 \\ R(x_{21}, \omega) & R(x_{22}, \omega) & & \\ \vdots & & \ddots & \vdots \\ 0 & & \cdots & R(x_{NN}, \omega) \end{pmatrix}. \tag{20}$$

2.4 Numerical aspects

One of the prerequisites of obtaining a valid outcome of the model is to have enough boundary sample points. In general there is the minimum requirement of satisfying Nyquist's spatial sample theorem. The expression for the maximum frequency in relation to the sample distance is given as:

$$f_{\max} = \frac{c}{2\Delta\xi} \tag{21}$$

with $\Delta\xi$ the distance between two boundary sample points.

3 Simulations

3.1 L-wall structure

A simple L-shaped wall geometry is taken, where a single broadband point source is placed in front and a microphone array in between as in Fig. 10. The wave field is simulated with both an angle independent reflection coefficient and an angle dependent reflection coefficient with a block function in the k_x-domain, as given in Fig. 9.

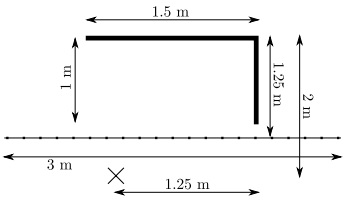

Figure 10: Geometry L-wall with source and detector array.

The results and differences are given in Fig. 11, where the following effects are visible: The edge diffraction of the wall ends (arrow a), first order reflection of the wall parallel to the detector array (arrow b) and the second order reflection of the sidewall to the parallel wall (arrow c). The first reflection does not show much difference, because the incoming wave field is in an almost perpendicular angle. So it reacts as a quasi locally reacting surface due to the block reflection coefficient function in the k_x-domain. On the other hand the second order reflection is a result of a wave field coming in under an angle. This explains the difference between the second order reflection and the first order reflection, caused by non-locally reacting boundary properties. Of course a block function for the reflectivity is an extreme case, in real materials the difference will be less. What can also be observed is the edge diffraction at the two ends of the wall in both cases and is similar for the locally and non-locally reacting case.

3.2 Rectangular box

A comparison is made between BEM and WRW in calculating the sound pressure in a rectangular box of dimensions $x = 0.21$ m, $y = 0.21$ m and $z = 0.03$ m. Inside, a point source is placed at (0.015, 0.015, 0.015) m and a detector at (0.21, 0.21, 0.03) m as given in Fig. 12. The results

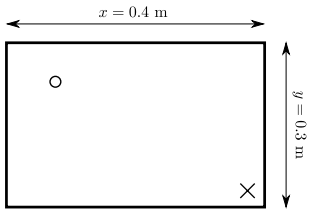

Figure 12: Rectangular box of height $z = 0.2$ m with source ($\times$) and detector ($\circ$).

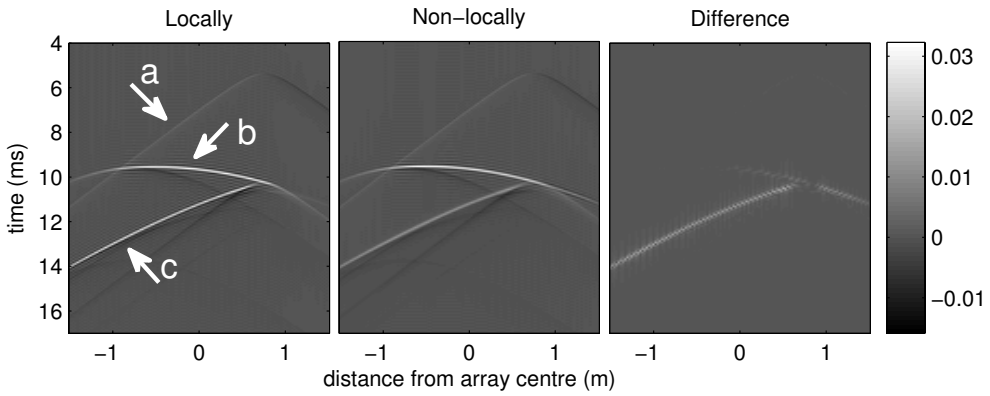

Figure 11: Reflected pressure fields (in Pa) of non-locally and locally reacting L-wall, and the difference.

are shown in Fig. 13 for the sound pressure amplitude and in Fig. 14 for its phase. In the WRW method occurs a small frequency shift, which could be due to the small dimensions of the box: The Rayleigh-II integral is based on infinite boundaries. The boundary influences for a larger box are way less than in this small box. In further research the differences for larger geometries will be investigated.

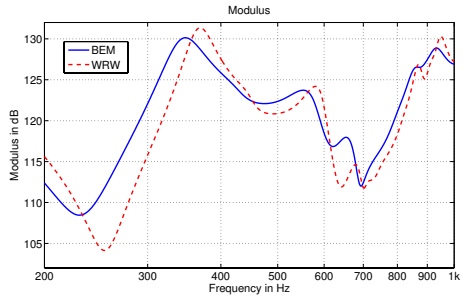

Figure 13: Sound pressure in point $x = 0.21$ m, $y = 0.21$ m and $z = 0.03$ m for BEM and WRW simulation.

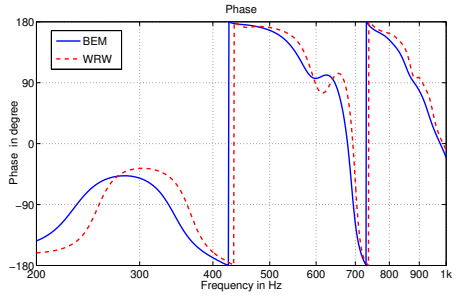

Figure 14: Phase in point $x = 0.21$ m, $y = 0.21$ m and $z = 0.03$ m for BEM and WRW simulation.

4 Conclusions

A 3-D acoustical simulation algorithm (WRW method) is presented, which is able to handle edge diffraction and non-locally reacting (angle dependent) boundary conditions. Preliminary results are shown for an L-wall shaped structure and a small rectangular box. It is necessary to further investigate the influence of non-locally reacting boundary properties on the total wave field compared to locally reacting ones. Furthermore, the cause of the differences between the BEM and WRW results shown in the frequency domain must be identified for the validity of the method in combination with the geometry considered.

Acknowledgements

This research was funded by the Deutsche Forschungsgemeinschaft (DFG) as part of the SEACEN research unit. Special thanks to Markus Müller-Trapet for the help with the BEM simulations.

References

[1] J. Borish, "Extension of the image model to arbitrary polyhedra", *J. Acoust. Soc. Am.* **75**(6), 1827-1836 (1984)

[2] A. Krokstad, S. Strøm, S. Sørsdal, "Calculating the acoustical room response by the use of a ray-tracing technique", *J. Sound Vib.* **8**(1), 118-125 (1968)

[3] M. Vorländer, "Simulation of the transient and steady-state sound propagation in rooms using a new combined ray-tracing/image-source algorithm", *J. Acoust. Soc. Am.* **86**(1), 172-178 (1989)

[4] U.P. Svensson, "Modelling acoustic spaces for audio virtual reality", *Proc. 1st IEEE Benelux Workshop on Model based Processing and Coding of Audio*, 109-116 (2002)

[5] B.-I. Dalenbäck, M. Kleiner, U.P. Svensson, "A macroscopic view of diffuse reflection", *J. Audio Eng. Soc.* **42**(10), 793-807 (1994)

[6] R.R. Torres, U.P. Svensson, M. Kleiner, "Computation of edge diffraction for more accurate room acoustics auralization", *J. Acoust. Soc. Am.* **106**(5), 2331-2344 (1999)

[7] A.D. Pierce, "Acoustics: An introduction to its physical principles and applications", *Acoustical Society of America, New York, 1991*, ch. 9

[8] U.P. Svensson, R.I. Fred, J. Vanderkooy, "An analytic secondary source model of edge diffraction impuls responses", *J. Acoust. Soc. Am.* **106**(5), 2331-2344 (1999)

[9] J. Baan, D. de Vries, "Reflection and diffraction in roomacoustic modelling", *Proc. Forum Acusticum*, Berlin (1999)

[10] M. Vorländer, "International round robin on room acoustical computer simulations", *Proc. 15th Intl. Congress on Acoustics (ICA)* Trondheim, **II**, 689-692 (1995)

[11] I. Bork, "A Comparison of Room Simulation Software - The 2nd Round Robin on Room Acoustical Computer Simulation", *ACUSTICA united with acta acustica* **86**(6),943-956 (1999)

[12] A.J. Berkhout, D.J. Verschuur, "Estimation of multiple scattering by iterative inversion, Part I: Theoretical considerations", *Geophysics* **62**(5), 1586-1595 (1997)

[13] A.J. Berkhout, "Applied Seismic Wave Theory", *Elsevier, Amsterdam, 1987*

[14] A.J. Berkhout, D. de Vries, J. Baan, B.W. van den Oetelaar, "A wave field extrapolation approach to acoustical modeling in enclosed spaces", *J. Acoust. Soc. Am.* **105**(3), 1725-1733 (1999)

[15] C.G.M. de Bruin, C.P.A. Wapenaar, A.J. Berkhout, "Angle-dependent reflectivity by means of prestack migration", *Geophysics* **55**(9), 1223-1234 (1990)